THE ATOMIC-SCALE CHARACTERIZATION OF DEFECTS ON CLEAVED VANADIUM AND MOLYBDENUM OXIDE SURFACES USING STM

GREGORY S. ROHRER AND RICHARD L. SMITH
Carnegie Mellon University
Department of Materials Science and Engineering
Pittsburgh PA 15213

ABSTRACT

Scanning tunneling microscopy (STM) was used to determine the structure of cleaved, single crystal surfaces of V_2O_5, V_6O_{13}, $Mo_{18}O_{52}$, and Mo_8O_{23}. Constant current images were recorded in ultrahigh vacuum and in air. By imaging well-defined surfaces that exhibit structural and chemical similarities, and comparing the observations to the known bulk structures, it is possible to establish a reliable interpretation for the contrast in the STM images. A comparison of images from the $V_6O_{13}(001)$ and the $V_2O_5(001)$ surfaces clearly shows that the surface V coordination polyhedra that are capped by vanadyl O can be distinguished from those that are not. This allows vacancies in the vanadyl O position to be identified on cleaved $V_2O_5(001)$ surfaces. $Mo_{18}O_{52}(100)$ and $Mo_8O_{23}(010)$ provide models for two different characteristic types of surface/crystallographic shear (CS) plane intersections. The shear in Mo_8O_{23} lies in the (010) surface plane and creates dark contrast along the [001]. The CS planes in $Mo_{18}O_{52}$, on the other hand, have components of shear both in and normal to the (100) surface plane and create white contrast parallel to [010]. These standards for contrast identification can be used to identify defects on inhomogeneous surfaces.

INTRODUCTION

There is a considerable body of experimental evidence supporting the idea that the oxidation reactions catalyzed by molybdenum and vanadium oxides are influenced by the atomic-scale structure of their surfaces and the defects that are present there [1-6]. However, the development of a mechanistic understanding of the relationship between the structure of a surface and its properties awaits detailed structural data. In general, both the periodic and the defective components of the surface structure must be characterized. The periodic characteristics of a compound surface include the composition and arrangement of the termination layer. The defective components include bulk planar and line defects that intersect the surface, point defects in the surface plane, and steps. Because the Mo and V oxides use lattice O to oxidize hydrocarbons, characterizing the population and configuration of defects such as O vacancies and crystallographic shear (CS) planes that mediate the reduction and re-oxidation processes is especially important.

The scanning tunneling microscope (STM) provides a unique opportunity to directly observe, in real-space, the components of the surface structure listed above. In contrast to more energetic surface structure probes, such as low energy electron diffraction, which have the potential to alter the labile molybdate [7] and vanadate [8] surfaces by promoting reduction reactions, the STM interacts only very weakly with the surface and does not alter its structure. The ability of the STM to image defect structures on inhomogeneous transition metal oxide surfaces has been clearly demonstrated in the past [9-12]. However, it can also be said that nonstoichiometry, structural complexity, uncertainties regarding the nature of the bonding, and the limited number of experimental precedents all make it difficult to establish unambiguous interpretations of observed image contrast. One of the goals of this paper is to demonstrate that

Mat. Res. Soc. Symp. Proc. Vol. 357 © 1995 Materials Research Society

by imaging several well-defined surfaces with related structures and comparing the observations to the known bulk structures, it is possible to establish reliable interpretations for high resolution STM images. Another goal is to demonstrate that defects such as O vacancies and surface/CS plane intersections can be distinguished in STM images of these important transition metal oxide surfaces.

In previous reports, we have compared the atomic-scale resolution STM images of chemically similar, but structurally different, alkali tungsten bronzes [13-14]. In this paper, we compare two related vanadates (V_2O_5 and V_6O_{13}) and two related molybdates ($Mo_{18}O_{52}$ and Mo_8O_{23}). The two molybdenum oxides investigated in this study have ordered CS planes that occur with a known concentration and orientation. Thus, they serve as experimental models to identify the contrast associated with surface/CS plane intersections. The two vanadates have closely related structures that are expected to terminate in different patterns. Comparing images of these different terminations allows us to determine the effect of singly coordinated O on the image contrast and what to expect from vacancies in this position.

EXPERIMENTAL

Single crystals of selected molybdate and vanadate phases were grown by chemical vapor transport reactions in sealed, evacuated, quartz ampoules. Black, platy crystals of $Mo_{18}O_{52}$ were grown by transporting stoichiometric mixtures of Mo and MoO_3 powders with I_2 at approximately 677 °C [15, 16]. Purple, equiaxed crystals of Mo_8O_{23} were also prepared from stoichiometric mixtures of Mo and MoO_3 powders. In this case, however, the reactants were annealed isothermally, for at least five days, at 690 °C, in the presence of I_2 vapor. Black platy crystals of V_6O_{13} were grown by transporting stoichiometric mixtures of V_2O_5 and V_2O_3 powders with $TeCl_4$ in a small temperature gradient around 600 °C [17]. Brown, lustrous crystals of $Na_{0.003}V_2O_5$ were grown by transporting $Na_xV_2O_5$ powder with $TeCl_4$ in a small temperature gradient near 530 °C [18]. In each case, the identity of the phase and the orientation of the crystal were established using conventional X-ray diffraction methods.

V_6O_{13}, $Mo_{18}O_{52}$, and Mo_8O_{23}, are all mixed valence compounds with sufficient electronic conductivity for the high resolution STM experiments. V_2O_5, on the other hand, is insulating when pure and not suitable for high resolution imaging. Its conductivity was, therefore, increased by intercalating a small amount of Na during the crystal growth. Because the Na resides in the interlayer spaces of the structure and donates an electron to the V_2O_5 framework, small concentrations increase the conductivity without altering the structure. The composition of the samples described in this paper, determined by flame emission spectroscopy, was $Na_{0.003}V_2O_5$. We have also found that dissolving Mo on the V site during growth increases the conductivity to levels suitable for STM imaging.

Surfaces were prepared for STM imaging by cleavage. $Mo_{18}O_{52}$ and V_2O_5 can be considered layered compounds. In other words, their three dimensional structures are composed of identical layers that are connected to each other only by weak van der Waals bonds. These compounds are easily cleaved using adhesive tape. Mo_8O_{23} and V_6O_{13}, on the other hand, have strong ionic-covalent bonds in all directions and must be cleaved with a razor blade. Because the bonding is anisotropic, the $Mo_8O_{23}(010)$ and the $V_6O_{13}(001)$ surfaces are easily exposed. The cleavage was carried out either in the ultrahigh vacuum (UHV) environment, in a N_2 filled glove bag attached to the vacuum chamber's load lock, or in air (after which the sample was either transferred to the UHV chamber via a load-lock or imaged in air). In one case, where all three preparations were tried on the same compound (V_2O_5), no substantive differences could be observed in the images recorded in UHV. We have found that reliable, atomic-scale imaging is only practical on very flat surfaces. Figure 1 shows an example of a cleaved surface that is ideally suited for high resolution imaging. In general, the cleaved surfaces examined in this study were characterized by large flat terraces separated by unit cell height steps along high symmetry directions. All of the high resolution images described in this paper were recorded on such terraces, far from steps.

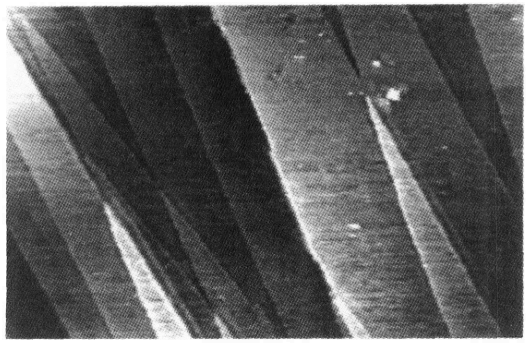

Figure 1. STM image of a 1.76 μm x1.33 μm x 50 Å area of a cleaved V_6O_{13}(001) surface, recorded in UHV. The sample bias was 2.8 V and the tunnel current was 0.8 nA.

The images reported here were made in the constant current mode with clipped Pt-Ir tips. The current and bias conditions used for each sample are specified in the image captions. The images presented here are representative of numerous observations and were selected based on resolution and consistency (irreproducible or infrequently observed contrast patterns are assumed to be artifacts of the tip structure). With the exception of Fig. 2c, which was recorded in air (images with comparable resolution have not yet been recorded in UHV), all images were recorded in UHV. A background plane has been subtracted from each image to remove the tilt that otherwise obscures atomic-scale features. The primary source of dimensional error in the images is thermal drift, which tends to distort the images in the slow scan direction (the top-to-bottom dimension). No thermal drift corrections have been applied. In some cases, high frequency noise, smaller than any of the recognizable periodic features in the image, has been removed.

RESULTS AND DISCUSSION

Contrast Interpretation

Before beginning a discussion of the observed contrast in the high resolution STM images, it is appropriate to consider the electronic structure of the compounds in question. The common features of these compounds are that they have a more than 2.0 eV band gap that separates a filled π band and an unfilled or partially filled π^* band that are formed by the overlap of O 2p and transition metal d orbitals [19]. The polarity of the compounds suggests that the anti-bonding π^* conduction band should have metal "d" character and the bonding π valence band should have "O 2p" character. The compounds examined in this study can all be described as n-type semiconductors, with a high concentration of shallow donors, or as semi-metals, with a small fraction of the π^* conduction band states occupied. In either case, the Fermi level is positioned near the bottom of the conduction band, more than 2 eV above the top of the occupied states in the valence band. Considering the range of biases used in our experiments, all images were formed by electrons tunneling to unoccupied conduction band states (positive sample biases) or from occupied conduction band states (negative sample biases). Therefore, all things being equal, we expect the tip to be more sensitive to the metal atom positions than the O atom positions. However, the relative geometric position of the metal and O atoms is also important. Tunneling occurs with a probability that has an inverse exponential relationship to the vertical position of the atoms (and the electronic states associated with them). Thus, adventitious positioning of the O atoms above the metal atoms

might increase the sensitivity of the tip to the O atoms and even reverse the contrast. In previous reports, we used a computational model to quantify the contributions of these two factors and to simulate the image contrast. Based on these simulations, we conclude that if the orbitals associated with the O atom positions make up 10 % of the conduction band density of states, and they are positioned more than 1 Å above the metal atoms, they will dominate the image contrast.

The considerations discussed above allow us to clearly distinguish between the two cases we encounter most frequently: a relatively flat surface composed of metal and O atoms at the bases of inverted square pyramids and a more corrugated surface terminated by singly coordinated apical O atoms that cap upright square pyramids or octahedra in an axial orientation. On the first surface, the contrast should be dominated by the metal atoms and on the second surface, it should be dominated by the apical O that eclipse the metal positions.

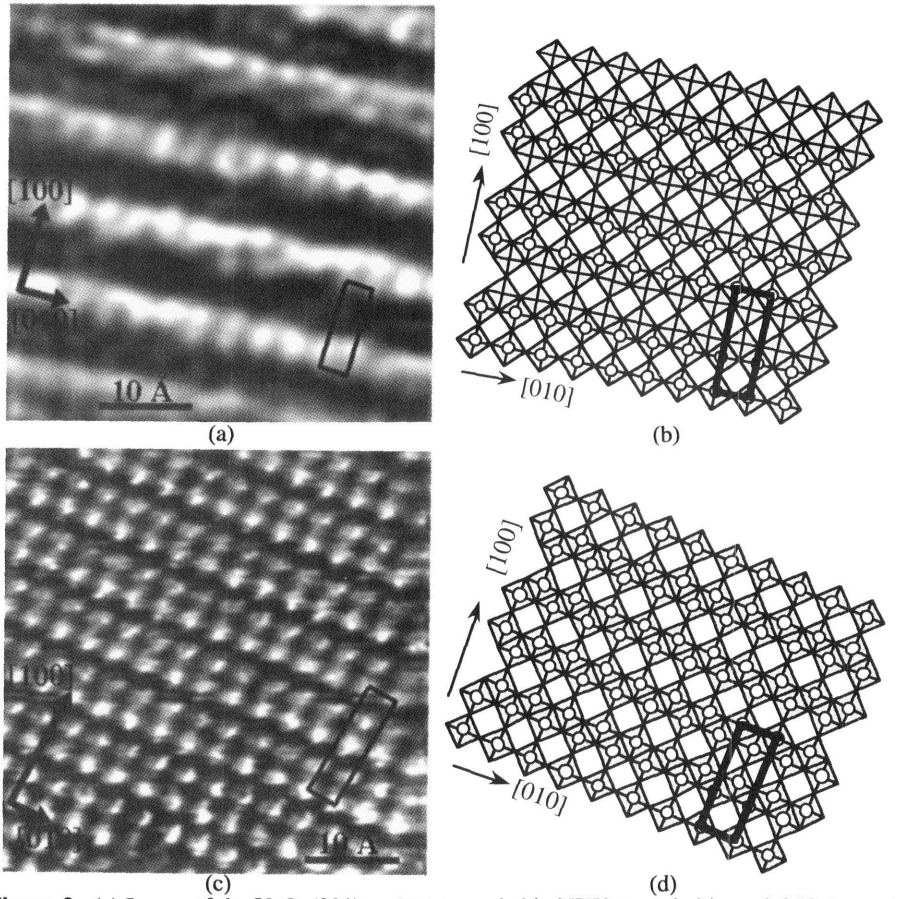

Figure 2. (a) Image of the $V_2O_5(001)$ surface recorded in UHV, sample bias = 2.0 V, current = 0.8 nA. Vertical distance from black-to white is 2.25 Å. The scale bar is 10 Å. (c) Image of the $V_6O_{13}(001)$ surface recorded in air, sample bias = -0.65 V, current = 1.3 nA. Vertical distance from black-to white is 1.5 Å. The scale bar is 10 Å. (b&d) Polyhedral structural models for the surface to the left (not to scale). See text for explanation.

The Vanadates

Representative STM images of the $V_2O_5(001)$ and the $V_6O_{13}(001)$ surfaces are shown in Fig. 2. Both images have a repeat unit that nearly matches the expected 1x1 dimensions for the (001) plane. Small differences, particularly in the slow scan direction, are caused by thermal drift. The contrast in the image of $V_2O_5(001)$ is dominated by lines of light and dark contrast that run parallel to [010]. The lines of lighter contrast are approximately 5 Å wide; they have an 11 Å period and a 2 Å corrugation. A smaller corrugation, within these lines of lighter contrast, has a periodicity of 3.6 Å and an amplitude of only 0.3 Å. The contrast in the image of $V_6O_{13}(001)$ is dominated by pairs of round white features arranged in staggered rows to form a centered rectangular pattern. The distance between the pairs is 3.6 Å along [010] and the vertical corrugation is approximately 1.5 Å. We can understand the contrast in these images by considering the bulk structures and our expectations for the way that they will cleave (see Fig. 3).

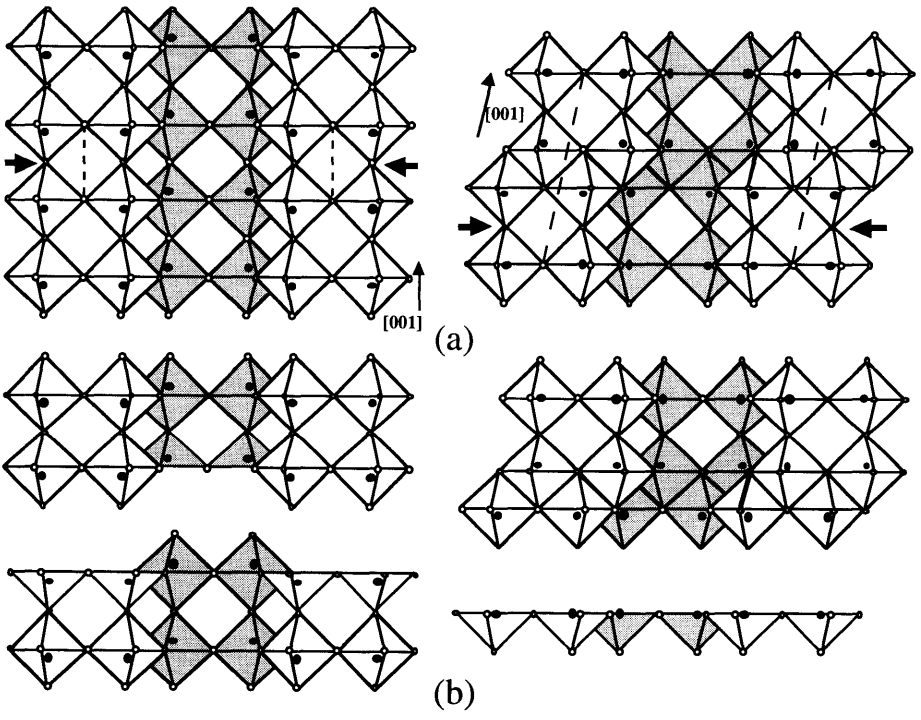

Figure 3. (a) The structural relationship between V_2O_5 (left) and V_6O_{13} (right) is shown in projection along [010]. The V atom positions are indicated by black circles and octahedral coordination by the O ligands is assumed. The shaded octahedra share edges with, and are in a plane behind, the unshaded octahedra. (b) Termination patterns produced by assuming that the longer, weaker bonds break along the plane indicated by the arrows in (a). See the text for description.

V_2O_5 (Pmmn, a = 11.52 Å, b = 3.56 Å, c = 4.37 Å) is the most highly oxidized vanadium oxide and V_6O_{13} (C2/m, a = 11.92 Å, b = 3.68 Å, c = 10.14 Å, β = 100.87°) is a

somewhat reduced form [20]. The structures of these two compounds are closely related by a crystallographic shear process which is thought to occur topotactically [8]; V_2O_5 transforms to V_6O_{13} by releasing O and shearing in the (001) plane to eliminate the vacancies. This relationship is illustrated in Fig. 3a. In the context of the results shown in Fig. 2, it is interesting to note the similarity of these structures in planes parallel to (001). First, the a and b cell lengths are nearly the same. Second, the planes of octahedral groups parallel to (001) exhibit the same linkages in both phases. Based on these similarities, we might expect the (001) surfaces of these two compounds to be the same. There are, however, important differences in the details of the cation coordinations.

In order to better illustrate the structural relationship between the two phases, Fig. 3 suggests that V is octahedrally coordinated in both phases. While this is true for V_6O_{13}, the V coordination in V_2O_5 would more accurately be described as square pyramidal. Because the V atoms occupy positions distorted far from the center of the octahedra, each "octahedron" has one very short axial bond (1.58 Å) and one very long bond (2.78 Å). While the short "vanadyl oxygen" bond has covalent character and is very strong, the long bond is very weak and would be best described as a van der Waals bond [21]. This creates an undulating pathway of weak bonds parallel to [001] that are expected to break during cleavage to produce the two identical surfaces shown in the left-hand portion of Fig. 3b. The surface plane, therefore, consists of a combination of inverted square pyramids and upright square pyramids capped with apical O atoms. The coordination around the V atoms in V_6O_{13}, on the other hand, is far more symmetric and this structure has no weak van der Waals bonds. This difference is obvious in the mechanical properties of the single crystals; the V_2O_5 crystals are soft and micaceous while the V_6O_{13} crystals are far more robust. Assuming a path that breaks the fewest and longest V-O bonds, the termination patterns shown in the right-hand side of Fig. 3b are produced by cleavage. Thus, the primary difference between the $V_2O_5(001)$ surface and these $V_6O_{13}(001)$ surfaces is that the $V_2O_5(001)$ is terminated by a mixture of O at the apices of upright square pyramids and V at the bases of inverted square pyramids, whereas the $V_6O_{13}(001)$ surface is terminated uniformly by one or the other structural feature. Thus, for the purposes of contrast interpretation, we need only distinguish between the planar bases of the inverted square pyramids and the upright square pyramids that place a vanadyl O 2 Å above the surface plane.

The models in Fig. 2b and 2d have been drawn to represent the surface structures proposed above. A projection onto the (001) plane of V_2O_5 shows pairs of corner-sharing V-O polyhedra that link along [010] by corners to form chains that link along [100] by edges. Half of the polyhedra, the upright square pyramids capped by an apical O atom, are labeled with a white circle. The other squares represent the bases of inverted square pyramids. V_6O_{13} has the same polyhedral linkages, as is illustrated in Fig. 2d, but all of the polyhedra are the same. They are either octahedra capped by an apical O (as indicated in the figure) or they are inverted square pyramids with a V atom exposed. Based on these proposed surface structures, we can explain the contrast in the observed STM images. The apical O atoms that cap every other pair of V-O polyhedra on the V_2O_5 surface protrude more than 2 Å from the surface plane and create the dominant white contrast parallel to [010]. The minor contrast along these rows is due to the spacing between these pairs. Thus, the upright square pyramids, capped by the apical O, dominate the image contrast because of their proximity to the tunneling tip. The knowledge that there is only one type of polyhedral bonding group (either inverted square pyramids or octahedra) on the $V_6O_{13}(001)$ surface allows us to conclude that each group should create the same image contrast. In fact, there is a one-to-one correspondence between the round white features in the experimental image and the positions of the V-O polyhedra. While it is not possible to unambiguously assign this contrast to the O at the apices of octahedral groups or to the V at the bases of the inverted square pyramids, we assume that, based on the magnitude of the corrugations and the stability of the surface in air, this is the O terminated surface.

The fact that we can easily distinguish between the upright and inverted square pyramids on the $V_2O_5(001)$ surface means that we also have the opportunity to distinguish O vacancies in the vanadyl O position. Because the vacancy converts an upright square pyramid to an inverted one, the defect should create a reduction in the vertical corrugation. Such reductions in the corrugation have been observed in images recorded in UHV. Three images

are shown for comparison in Fig. 4. The images labeled (a) and (b) were recorded from the same surface and exhibit the same periodicities. However, the vertical corrugation in (a) is 2.25 Å while the vertical corrugation in (b) is less than 1.0 Å. Furthermore, the rows of white contrast that dominate the image in Fig. 4a appear to be absent and only the minor corrugation remains. The images in Figs. 4a and b were selected as nearly homogeneous examples of two limiting cases for the contrast: those with large corrugations, as in (a), and those with small corrugations, as in (b). The image in Fig. 4c, displayed with 2.25 Å of vertical contrast, is representative of the inhomogeneous areas that were also observed. The inhomogenous areas, very common in larger-scale images, are characterized by low corrugation regions that exist (and are stable over many scans) between the broken lines of white contrast along the [010] axis.

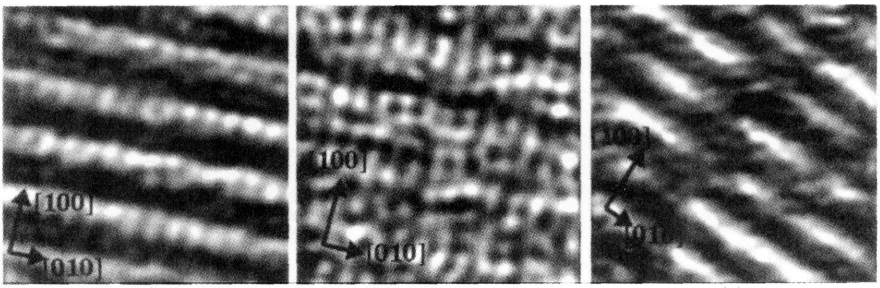

(a) (b) (c)

Figure 4. Three images of the $V_2O_5(001)$ surface recorded in UHV. (a) is identical to Fig. 2(a). (b) and (c) were recorded under similar bias and current conditions. (a) and (b) are 50 Å x 50 Å areas, (c) covers a 55 Å x 55 Å area. The vertical range from black-to-white is 2.25 Å in (a) and (c); it is 1.0 Å in (b). Sample bias = 2.0 V and current = 0.8 nA.

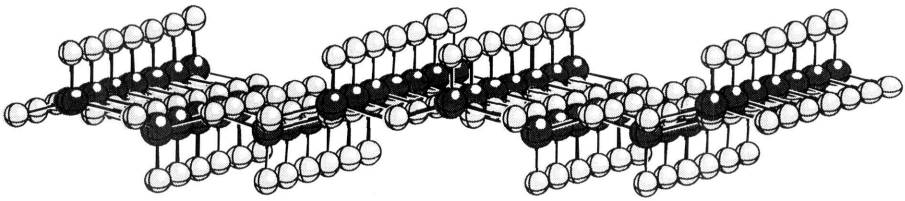

Figure 5. An oblique projection of the $V_2O_5(001)$ surface. The V are the darker spheres and the O are the white spheres. The vanadyl O protrude upward from the surface. Vacancies in these spots significantly reduce the surface corrugation.

Because the high and low contrast areas can be observed in the same images, we conclude that the contrast difference is due to a difference in the surface structure rather than a difference in the structure of the tip. Considering the model for the surface structure shown in Fig. 5, it is clear that vacancies in the vanadyl O position would lead to a reduction in the geometric corrugation of the surface. Thus, the most likely explanation is that the low corrugation regions in Fig. 4c correspond to regions where the singly coordinate surface O have been removed, the image in 4b shows an area where most or all of these atoms are missing, and the image in 4a is of a region where most of the O are intact. This interpretation is based entirely on geometric consideration, it is assumed that electronic effects play a subordinate role. The validity of this assumption was demonstrated by contrast simulations described in an earlier publication; the fact that the upright square pyramids are 2 Å closer to the tip overwhelms the fact that there is a lower density of states at this position [18].

STM observations of O disorder on transition metal oxide surfaces are not unprecedented [9-11]. However, the earlier cases involved crystals that were heated in vacuum, conditions where oxygen vacancy formation is expected. In this experiment, the surfaces were prepared by room temperature cleavage, so the disorder must be a result of the cleavage process or the STM measurement itself. Because the observed defect structure is stable during continuous scanning, we believe that the vacancies are created during the cleavage process rather than by the STM measurement. Although cleavage induced termination layer variations have been observed for compounds with three dimensional bonding [13], they are not expected to occur in compounds with a van der Waals gap. However, when one considers the physical and chemical properties of vanadium pentoxide, the observation of an oxygen deficient surface is not too surprising. The energy for the formation of a bulk oxygen vacancy, according to the reaction (in the standard Kröger-Vink notation):

$$O_O = V_O^{\bullet\bullet} + 2e' + 1/2\ O_2\ (g)$$

is known to be 1.3 eV, which makes it one of the most easily reduced transition metal oxides [22]. The fact that O is removed from the lattice with relative ease is, of course, related to the ability of V_2O_5 to catalyze the partial oxidation of hydrocarbons. In fact, it has been previously suggested that these vacancies play a role in the process [23]. Thus, by further characterizing the defect structure of this surface using real-space STM measurements, it should be possible to determine how the structure and properties of this surface are related.

The Molybdates

The two molybdenum oxides used in this study contain ordered arrangements of CS planes and a predictable CS plane/surface intersection pattern. Representative STM images of the $Mo_{18}O_{52}(100)$ and the $Mo_8O_{23}(010)$ surfaces are shown in Fig. 6a and 6c. Both images have a repeat unit that nearly matches the expected 1x1 dimensions for the surface plane, assuming a bulk termination. Comparing the images to the bulk structures allows us to identify the contrast associated with the surface/CS plane intersections.

The two molybdates can be described as deriving from two different fully oxidized MoO_3 structures by crystallographic shear (CS). $Mo_{18}O_{52}$ ($P\bar{1}$, a = 8.145 Å, b = 11.89 Å, c = 21.23 Å, α = 102.67°, β = 67.82°, and γ = 109.97°) is a layered compound derived from the layered α-MoO_3 structure by CS of $\frac{1}{2}\langle 1\bar{1}0\rangle\{35\bar{1}\}$ and Mo_8O_{23} (P2/a, a = 16.88 Å, b = 4.052 Å, c = 13.39 Å, β = 106.19°) is a three dimensionally bonded compound that is derived from the β-MoO_3 structure by CS of $\frac{1}{2}\langle 110\rangle\{\bar{1}20\}$ [24-26]. As is illustrated in Fig. 7, the $Mo_{18}O_{52}(100)$ and $Mo_8O_{23}(010)$ planes are analogous to the (010) planes of α- and β-MoO_3, respectively. While these planes would be nearly indistinguishable in the fully oxidized compounds (see Fig. 7a), they are very different in the reduced structures because of the CS planes that intersect the surface (see Fig. 7b and 7c). Specifically, the shear operation transforms the planar corner-sharing network into a mixture of corner and edge-sharing and in the $Mo_{18}O_{52}$ structure, moves a small fraction of the octahedrally coordinated Mo atoms to tetrahedral positions.

There are, however, two key differences between these structure. The first is that $Mo_{18}O_{52}$ is a layered compound and like V_2O_5, it has a well defined planar network of weak van der Waals bonds that break during cleavage (see Fig. 7d). These bonds are so weak that like V_2O_5, it can be cleaved with tape. Therefore, we know that the surface is terminated by singly coordinate O atoms at the apices of the Mo-O octahedra. Furthermore, because only weak bonds are broken during the cleavage, the surface is unlikely to reconstruct. Mo_8O_{23}, on the other hand, has strong ionic-covalent bonds in all three directions that must be broken

during the cleavage process (see Fig. 7e). The second significant difference is that the shear components that are integral to the Mo_8O_{23} structure lie in the plane of the surface and do not create any surface relief. Thus, edge-sharing octahedra in the surface plane are created, as shown in Fig. 7c. The shear operation integral to the $Mo_{18}O_{52}$ structure, on the other hand, has a component normal to the surface so the Mo-O octahedra share edges out of the plane of the surface and there is a small step (1.5 Å) at each surface/CS plane intersection, as shown in Fig. 7d. By comparing the bulk structures and the observed surface images, it is possible to see how these structural differences influence the contrast in STM images.

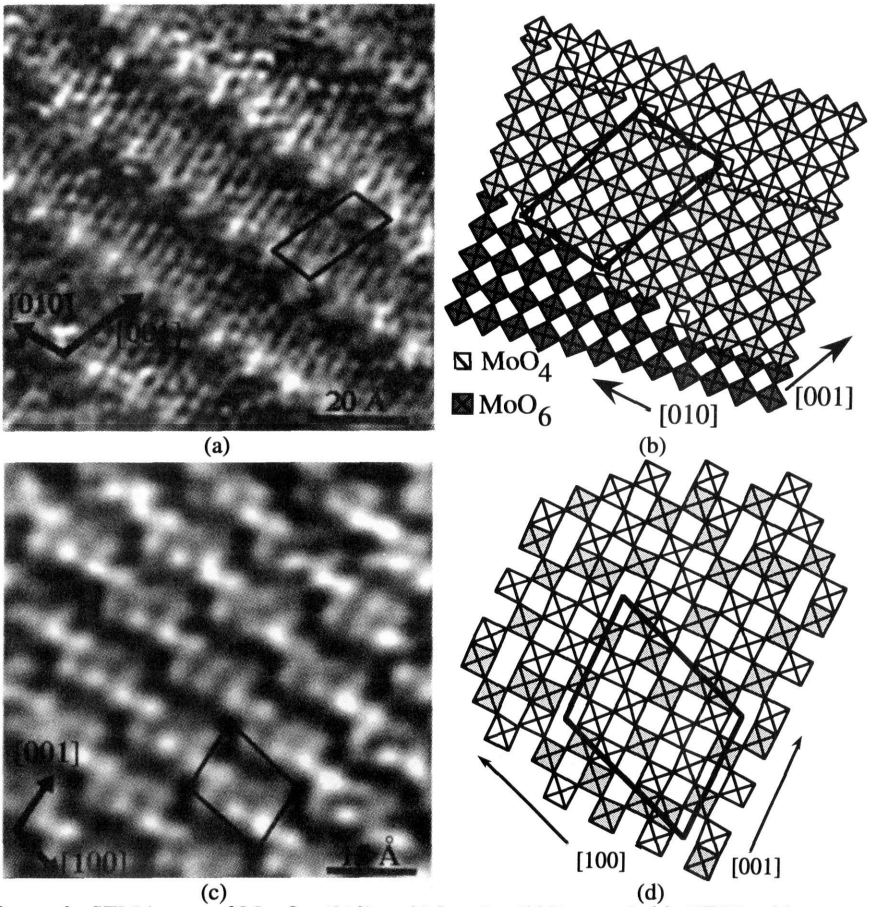

Figure 6. STM image of $Mo_8O_{23}(010)$ and $Mo_{18}O_{52}(100)$ recorded in UHV, with structural models. (a) 110 Å x 110 Å image of $Mo_{18}O_{52}(100)$; sample bias = -1.65 V; current = 0.7 nA; vertical scale from black-to-white is 2.5 Å, the scale bar is 20 Å (c) 75 Å x 75 Å image of $Mo_8O_{23}(010)$; sample bias = 1.3 V; current = 1.0 nA; vertical scale from black-to-white is 1.0 Å, the scale bar is 15 Å. The octahedra in (b) are shaded according to their relative height. Those in (d) are shaded according to the relative axial position of the Mo atom (see text for description).

We consider first the $Mo_{18}O_{52}$ (100) surface. Assuming that the surface cleaves at the van der Waals gap and that there is no significant rearrangement, we can interpret the contrast in terms of the known bulk crystal structure. The primary contrast is caused by a series of steps and terraces oriented along the [010] direction with a 26 Å period. There is also a series of bright features at the edge of each step which has an 11.8 Å average frequency along the direction of the step. The topographic variation over these features is less than 1.0 Å. There is also a series of rows within each step which have a periodicity of 3.8 Å and a corrugation height of 0.4 Å. Any additional features within these rows are incompletely resolved. Based on their spacing and orientation with respect to other features, we assign the lines of contrast with the 26 Å periodicity to the surface/CS plane intersections that define the boundaries of the unit cell. Between the CS planes, the structure of $Mo_{18}O_{52}$ is nearly identical to MoO_3. Each of these "MoO_3-like" terraces in the model in Fig. 6b is shaded differently to indicate that they are at different vertical positions. Using the bulk structure as a model, the vertical displacement between two terraces separated by a surface/CS plane intersection should be 1.7 Å. Measured vertical displacements on the image vary from 1.5 to 2.5 Å, depending on the point of measurement.

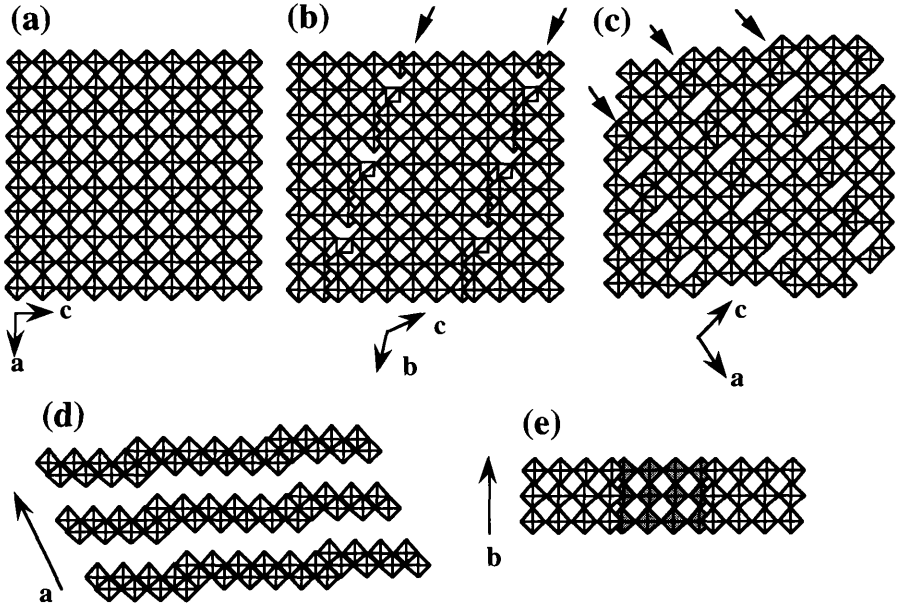

Figure 7. The relationship between the MoO_3, $Mo_{18}O_{52}$, and Mo_8O_{23} structures. (a) A single layer of the (010) plane of the α- and β-MoO_3 is essentially the same. Shearing (along lines indicated by the arrows) in two different ways leads to edge-sharing configurations out of the plane (b) and in the plane (c). These are the $Mo_{18}O_{52}$, and Mo_8O_{23} structures, respectively. Views parallel to the surface plane show that $Mo_{18}O_{52}$ (d) has weak bonds between the layers while Mo_8O_{23} (e) has strong bonds holding the layers together.

The 3.8 Å period of the contrast within the terraces correlates with both the positions of the Mo atoms and the apical O atoms that cap the MoO_6 octahedra. Although we expect the apical O to dominate the contrast due to its closer proximity to the tunneling tip, we will simply assume that it is the MoO_x group as a whole that is responsible for the contrast. This

interpretation is consistent with explanations of the contrast in STM images of alkali molybdate bronzes, related compounds which can also be considered as arrangements of MoO_x polyhedra [27-29]. Thus, we assign the 3.8 Å periodicity to the rows of corner sharing MoO_6 octahedra in each terrace (see Fig. 6b). This assignment leads to an explanation of the bright contrast that occurs with an 11.8 Å period at the end of every third row of octahedra. The position and frequency of these spots correspond to the only positions on the surface where MoO_4 tetrahedral units occur. One possible reason for the pronounced contrast difference between the tetrahedral and octahedral units, based solely on geometric considerations, is that while a Mo atom in the octahedral environment is well shielded from the tip by the apical oxygen, in the tetrahedral unit there is a direct line between it and the tip which might lead to an enhanced local density of electronic states and the enhanced corrugations. In any case, the two coordination polyhedra are clearly discriminated.

The contrast in the STM image of $Mo_8O_{23}(010)$ is dominated by narrow lines of black contrast that run parallel to [100] and kink every 16.78 Å. The lines are separated by 13.57 Å wide regions of white contrast. The white contrast regions are further broken up into 3 sub-units. The vertical variations on this surface are all less than 1 Å. Since these lines of dark contrast have the perodicity and orientation of the CS plane/surface intersection, we conclude that these are the shear plane positions. It is interesting to note that when there is a vertical step at the CS plane/surface intersection, as for $Mo_{18}O_{52}$, the geometric effect creates a line of white contrast. However, when there is no topographic elevation, the shear planes create lines of dark contrast. This implies that the electronic density of states is diminished at these positions, possibly because the greater density of cations along these planes traps some charge and reduces the density of the unfilled orbitals that we are probing.

Some aspects of the contrast are not easily explained. For example, according to the bulk model, the shear plane kinks should occur with a spatial frequency of a/2, rather than a. Also, there is no simple explanation for the region of white contrast between the shear planes to break up into three separate units. These contrast effects are probably related to the details of the termination layer and the relaxations that occur there. Unlike $Mo_{18}O_{52}$, there is no van der Waals gap and the termination pattern can not be known with certainty. Furhtermore, unlike V_6O_{13}, which also has strong 3-dimensional bonding, we do not expect a uniform termination. The Mo atoms occupy positions that are displaced from the center of the octahedron along [010], forming one longer (2.4 Å) and one shorter (1.7 Å) axial bond. Assuming the longest (weakest) of the two bonds breaks, we can differentiate two types of polyhedra on the surface, inverted and upright square pyramids that are terminated by apical O. These octahedra have been given opposite shades in Fig. 6d to indicate this difference. Although this differentiation demonstrates that the two shear plane kink positions in the unit cell have different contiguous environments, it does not explain why one is imaged as a dark spot and the other is not. It is hoped that further imaging experiments and contrast simulations will resolve this issue.

CONCLUSION

Atomic-scale resolution STM observations of selected Mo and V oxide surfaces have been discussed in terms of the bulk structures of the compounds. Through such comparisons, it is possible to assign contrast in the images to specific surface features such as vanadyl O, O vacancies, and surface/CS plane intersections. These particular structural features are of interest because CS planes and O vacancies mediate the redox processes in the materials. Thus, they are expected to be present on the surface of a working oxidation catalyst. Such a surface is expected to have an inhomogeneous structure and a composition intermediate between the fully oxidized forms (MoO_3 and V_2O_5) and the stable reduced phases. By establishing procedures for imaging these compounds at high resolution, and precedents for the interpretation of the image contrast, we hope to enable future studies of more complex surfaces.

ACKNOWLEDGMENTS

This work was supported by the National Science Foundation under YIA Grant DMR-9458005. R. L. S. thanks the NSF Research Experiences for Undergraduates program.

REFERENCES

[1] J. E. Germain, in Adsorption and Catalysis on Oxide Surfaces, edited by M. Che and G. C. Bond (Elsevier, Ansterdam, 1985) p. 355.
[2] J. Haber, in Solid State Chemistry in Catalysis edited by R. Grasselli and J. Brazdil (American Chemical Society, Washington D.C., 1985) p. 1.
[3] M. K. Smith and U. S. Ozkan, J. Catalysis **141**, 124 (1993).
[4] R. L. McCormick and G. L. Schrader, J. Catalysis **113**, 529 (1988).
[5] S. Barber, J. Booth, R. D. Pike, R. Reid, R. J. D. Tilley, J. Catalysis **77**, 180 (1982).
[6] W. E. Farneth, E. M. McCarron III, A. W. Sleight, R. H. Staley, Langmuir **3**, 217 (1987).
[7] L. E. Firment and A. Ferrretti, Surface Science **129**, 155 (1983).
[8] M. N. Colpaert, P. Clauws, L. Fiermans, and J. Vennik, Surface Science **36**, 513 (1973).
[9] G. S. Rohrer, V. E. Henrich, D. A. Bonnell, Science **250**, 1239 (1990).
[10] P. W. Murray, F. M. Leibsle, H. J. Fisher, C. F. J. Flipse, C. A. Muryn, G. Thornton, Phys. Rev. B **46**, 12877 (1992).
[11] T. Matsumoto, H. Tanaka, T. Kawai, S. Kawai, Surface Science Letters **278**, L153 (1992).
[12] G. Tarrach, D. Bürgler, T. Schaub, R. Wiesendanger, H. J. Güntherodt, Surface Science **285**, 1 (1993).
[13] W. Lu, N. Nevins, M. L. Norton, and G. S. Rohrer, Surface Science **291**, 395 (1993).
[14] G. S. Rohrer, W. Lu, M. L. Norton, M. A. Blake, C. L. Rohrer, J. Solid State Chem. **109**, 359 (1994).
[15] G. S. Rohrer, W. Lu, R. L. Smith, and A. Hutchinson, Surface Science **292**, 261 (1993).
[16] O. Bertrand, N. Floquet and D. Jacquot, J. Crystal Growth **96**, 708 (1989).
[17] K. Nagasawa, Y. Bando, T. Takada, J. Crystal Growth **17**, 143 (1972).
[18] R. L. Smith, W. Lu, and G. S. Rohrer, Surface Science, in press.
[19] J. B. Goodenough, in Progress in Solid State Chemistry, Vol. 5, edited by H. Reiss (Pregamon Press, Oxford, 1972) p. 145.
[20] K.-A. Wilhelmi, K. Waltersson, L. Kihlborg, Acta Chem. Scand. **25**, 2675 (1971).
[21] J. Y. Kempf, B. Silvi, A. Dietrich, C. R. A. Catlow, B. Maigret, Chem. Mater. **5**, 641 (1993).
[22] P. Kofstad, Nonostoichiometry, Diffusion, and Electrical Conductivity in Binary Metal Oxides (R. E. Krieger, Malabar, FL, 1983) p. 57.
[23] L. Fiermans, P. Clauws, W. Lambrecht, L. Vandenbroucke, J. Vennik, Phys. Status Solidi(a) **59**, 485 (1980).
[24] L. Kihlborg, Ark. Kemi. **21**, 443 (1963).
[25] L. Kihlborg, Ark. Kemi. **21**, 461 (1963).
[26] L. Kihlborg, Ark. Kemi. **21**, 471 (1963).
[27] J. Heil, J. Wesner, B. Lommel, W. Assmus, and W. Grill, J. Appl. Phys. **65**, 5220 (1989).
[28] E. Garfunkel, G. Rudd, D. Novak, S. Wang, G. Ebert, M. Greenblatt, T. Gustafsson, and S. H. Garofalini, Science **246**, 99 (1989).
[29] U. Walter, R. E. Thomson, B. Burk, M. F. Crommie, A. Zettl, and J. Clarke, Phys. Rev. B **45**, 11474 (1992).